

## Time-resolved tomographic PIV investigation of multichannel swirling jets

Fulvio Scarano<sup>1,\*</sup>, Andrea Ianiro<sup>2</sup>, Kyle Lynch<sup>1</sup>, Gennaro Cardone<sup>3</sup>

<sup>1</sup> Department of Aerospace Engineering, TU Delft, Delft, The Netherlands

<sup>2</sup> Aerospace Engineering Group, Universidad Carlos III de Madrid, Leganés, Spain

<sup>3</sup> Dipartimento di Ingegneria Industriale, University of Naples 'Federico II', Naples, Italy

\*corresponding author: f.scarano@tudelft.nl

---

**Abstract** The unsteady three-dimensional flow organisation of swirling jets issued from a nozzle at Reynolds number  $Re = 1,000$  and swirl numbers  $S$  ranging between 0.2 and 0.6 is investigated with time-resolved tomographic Particle Image Velocimetry. The instantaneous flow structure and its evolution are visualized using the vortex detection Q-criterion.

The time average flow structure indicates that the vanes used to impart the swirling motion have a significant impact on the azimuthal modulation of momentum with the jet exhibiting four sectors separated by a thin cross-like wake resulting from the boundary layer developed along the vanes walls. The flow field thus exhibits inner and outer shear regions. An increase in swirl is followed by a larger jet spreading angle. Further increase beyond  $S = 0.6$  causes the formation of a central recirculation zone due to vortex breakdown.

The swirling motion promotes the instability and helical vortices deform the outer axial shear layer as generated by Kelvin-Helmoltz waves, then penetrate towards the jet axis. The downstream evolution of the shear layer shows also the vortex pairing, which is not axisymmetric since the vortices undergo pairing alternatively in the inner and in the outer shear layer.

**Keywords:** swirling jets, PIV, tomography, vortex pairing, precessing vortex core

---

### 1 Introduction

Swirling flows frequently occur in nature and they are used in a wide variety of industrial applications. In gas turbine combustors, swirling jets generate reverse flow regions near the jet nozzle to stabilize the flame (Lilley, 1977, Candel et al. 2014). A swirling jet is obtained by imparting azimuthal momentum to an axial jet flow using a swirl generator, such as vanes (Harvey 1962), axial-tangential fluid entry (Chigier and Chervinsky 1967), rotating inlet tubes (Billant et al. 1998), or rotating perforated plates (Rose 1962). The monograph by Gupta et al (1984) covers swirl flows extensively. The swirling motion is demonstrated to affect both mean flow field properties and the unsteady large-scale organization. In the case of inert jets the degree of swirl imparted to the flow was reported to strongly influence the jet growth and entrainment rates as well as the turbulence decay process. The degree of swirl is quantified by the swirl number  $S$ , the ratio between the axial flux of swirl momentum and the axial flux of axial momentum times equivalent nozzle radius.

Jet growth, entrainment, and centreline velocity decay are all enhanced as the swirl number increases (see e.g., Park and Shin, 1993). Two distinct regimes are noted: low swirl ( $S < 0.5$ ), and high swirl ( $S > 0.5$ ). In the latter case, the stronger adverse pressure gradient determines the near field development of the jet along radial and axial directions, in turn leading to a flow recirculation zone close to the nozzle exit and associated to the vortex breakdown (Harvey, 1965). The latter remains of great interest for flame stabilization as demonstrated in the study of Lucca-Negro and O'Doherty (2001).

The unsteady flow organization of swirling jets develops under the effect of a shear layer composed of both azimuthal and axial components of shear. At sufficiently high Reynolds number, the azimuthal component of the shear layer introduces shear-induced instabilities of Kelvin-Helmholtz type similar to those encountered in non-swirling jets. Chanaud (1965) first observed three-dimensional oscillations in the jet structure. Subsequently Syred & Beér (1974) hypothesized a non axis-symmetric flow regime. Quantitative analysis was made with laser-doppler anemometry (LDA) by Yazdabadi et al. (1994) on a high swirl cyclone confirming that the reverse flow region displaces the central vortex core leading to the precessing vortex core

(PVC, Syred 2006). The LDA and PIV experiments by Martinelli et al. (2007), demonstrated the relation between the amplitude of the periodic PVC fluctuations and the Reynolds and swirl number. Liang and Maxworthy (2005) investigate vortical features in centrifugally unstable swirling jets at  $Re = 1,000$  with flow visualization and planar PIV.

Cala et al. (2006) identified three precessing spiral vortex structures in a model burner: a primary vortex that corresponds to the precessing vortex core, an inner secondary vortex, and outer secondary vortex, where the PVC is the most powerful structure associated to the dominant vorticity generated by the swirler.

Several other works (Oberleithner et al., 2011 and Markovich et al. 2014) have reconstructed the 3D oscillatory flow pattern from planar PIV snapshot using Proper Orthogonal Decomposition and showed that the flow field is characterized by a single global mode characterized by one dominant frequency.

Vortex pairing and the vortex core breakdown do not exhibit a specific plane of symmetry and past works (Ceglia et al. 2014) have concluded that comprehensive studies of the vortex dynamics would require the instantaneous measurement of velocity and vorticity field in a three-dimensional domain such as possible with tomographic PIV (Elsinga et al., 2006). The use of time-resolved tomographic PIV to describe jets without swirl at moderate Reynolds number was demonstrated in the work by Violato and Scarano (2011).

The present work describes the instantaneous three-dimensional organization and dynamical evolution of swirling jets produced by swirl vanes. The emphasis is put on the instantaneous vortex topology and the relation between the outer shear layer dynamics (Kelvin-Helmholtz vortices, their pairing and further breakdown) and the inner region where the precessing vortex core is active at higher values of the swirl number.

As tomographic PIV gives access to the instantaneous velocity field in a three-dimensional domain, the vorticity vector is represented in all its components along with the vortex detection criterion based upon velocity gradient tensor eigenvalues (Q-criterion, Hunt et al. 1988, Jeong and Hussain 1995).

Furthermore as surveyed in Scarano (2013), time-resolved three-dimensional measurements have been coupled with advanced data evaluation techniques (Sequential Motion Tracking Enhancement, Lynch and Scarano, 2015; Fluid Trajectory Correlation, Lynch and Scarano, 2014), which significantly improve measurement accuracy in terms of spatial resolution and velocity dynamic range.

## 2 Experimental apparatus and procedure

Flow field measurements are performed in the Jet Tomographic Facility (Violato et al. 2012) at the Aerodynamics Laboratories of TU Delft in the Aerospace Engineering Department. The experimental apparatus is sketched in Fig. 1a. A vertical swirling jet (with a nozzle diameter of 19.7 mm) emerges from the bottom wall of the facility: an octagonal water tank (600mm of inner diameter and 800mm of height) allowing full optical access for illumination and tomographic imaging. Neutrally buoyant polyamide particles with median diameter of  $56\mu\text{m}$  (VESTOSINT® 2157) are employed as seeding particles at a concentration of about 0.3 particles/ $\text{mm}^3$ .

The nozzle geometry is detailed in Fig. 1b. The swirling flow is imparted by four helical inserts (swirl vanes) in a cylindrical nozzle. The swirl number is varied in the range from 0 to 0.8. Results are here for  $S = \{0.2, 0.4, 0.6\}$ . The experiments are performed at  $Re = 1,000$  with an exit velocity of 0.05 m/s.

The tomographic PIV setup is sketched in Fig 1a. Illumination is provided by a solid-state diode-pumped Quantronix Darwin-Duo Nd-YLF laser (2x 25 mJ @ 1000 Hz). The laser beam with exit diameter of 6 mm is expanded with a diverging lens to a diameter of 8 cm and then focused with a converging lens towards the nozzle exit, in order to have a quasi-cylindrical illumination volume with a diameter of about 50 mm at the top of the measurement domain and 45 mm at the nozzle exit.

The light scattered by tracers is recorded by three 3 LaVision Imager Pro HS CMOS cameras (2016 x 2016 pixels, with 11  $\mu\text{m}$  pitch) subtending a planar angle of 90 degrees. Nikon objectives of 105 mm focal length are set with a numerical aperture  $f/\# = 22$  to allow focused imaging of the illuminated particles over the illuminated domain. For the chosen illumination and imaging configuration the maximum particle image density is approximately 0.04 particles/pixel at the jet axis.

The field of view has a digital resolution of 18.6 pixels/mm (pixel image size 53.75  $\mu\text{m}$ ). The measurement domain extends for 98 mm along the axial direction and 50 mm in the radial one. Sequences of 200 images are recorded at 100 Hz, providing imaged particle displacement of approximately 10 pixels at the jet exit, which enables time-resolved measurements and advanced data analysis based on sequences.

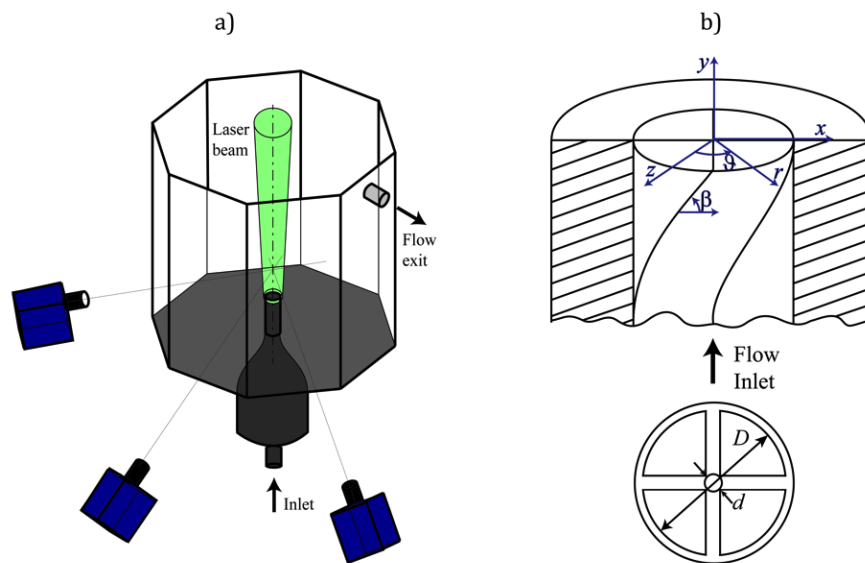


Fig. 1 Sketch of the experimental setup: a) Overall view of jet tomography facility with illumination and imaging. b) Detail of the swirling nozzle.

The calibration mapping function is obtained with a double-layered dot pattern and is corrected by the volume self-calibration technique (Wieneke 2008) to minimize registration errors to below 0.1 pixels. Background image intensity is reduced by image pre-processing (sliding minimum subtraction over a neighbourhood kernel of 31x31 pixels). The volumetric light intensity is reconstructed with an advanced technique that combines the multiplicative algebraic reconstruction technique (MART, Herman and Lent 1976) algorithm with the motion tracking enhancement (MTE, Novara, Batenburg & Scarano 2010) within a sequence-marching approach (SMTE, Lynch and Scarano, 2015). The voxel resolution is equivalent to the pixelwise applying a unity pixel to voxel ratio. The overall measurement volume is approximately  $43 \times 43 \times 86 \text{ mm}^3$  discretized with  $800 \times 800 \times 1600$  voxels.

The three-dimensional particles motion analysis is performed with the fluid trajectory correlation approach (FTC, Lynch and Scarano, 2013). A short sequence of 5 objects is used to reproduce the particles pattern motion, which is modelled with a 2nd order polynomial fit. The interrogation volume size is  $40 \times 40 \times 40$  voxels ( $2.1 \times 2.1 \times 2.1 \text{ mm}^3$ ). The overlap between adjacent interrogation boxes of 75% leads to a vector pitch of 0.5 mm (0.025 D).

### 3.1 Low-swirl jet organization

At  $S = 0.2$  the main coherent structures have the shape of helices. These vortices do not feature ring-like shape but more of a helix that surrounds the outer part of each jet section (Fig. 4 a). Helical structures have been described by Liang and Maxworthy (2005). The helix advances axially in the direction opposite to that of the swirl. The spacing between two subsequent vortices is approximately  $0.55 D$ . However the pitch of the helix is about  $1.1 D$ , which indicates a double helix arrangement of vortices that wraps each jet.

The helical vortices take their inception directly after the nozzle exit near the location of the maximum of axial velocity (Fig. 4 b), and surround the external shear layer of the jet. In the first part of the jet, the helix is interrupted in the interior region. As the jet evolves downstream, these vortical features seem to penetrate also towards the centre of the jet.

Vortex pairing is observed to occur after approximately three diameters. The resulting structure emerging after pairing exhibits not only a stronger circulation but also an increased azimuthal coherence. The vortices pair alternately in the external and in the internal part of the jet shear layer. Before pairing, the following

helical vortex undergo pronounced tilting with the most exterior (interior) portion of the vortex being lifted upwards more rapidly than the interior (exterior) one. The subsequent paired vortices feature a horse-shoe shape with the head region retarded (lifted) with respect to the legs. Further away from the exit, the topology of vortex filaments becomes more complex and irregular. Nevertheless vigorous horse-shoe vortices are observed with a periodic behaviour in the space between individual sectors.

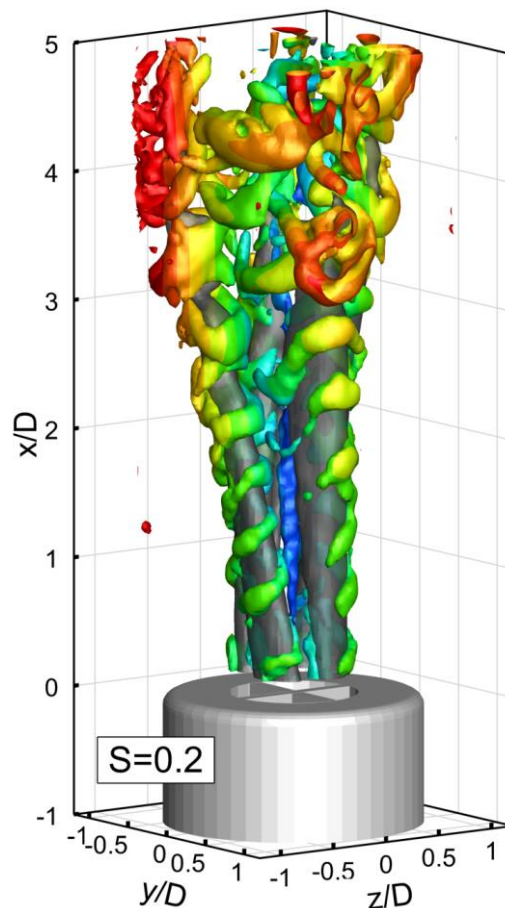


Fig. 2 Instantaneous flow field at  $S = 0.2$ . Isosurfaces of axial velocity ( $u/U = 0.7$ , dark gray) and of Q-criterion (color coded with radial distance from the jet axis).

At  $S = 0.4$ , the vortices formed at the outer edge of the jet sectors undergo pairing approximately two diameters downstream of the nozzle exit and produce vigorous rib-like vortices. The latter interconnect among the adjacent sectors. Differently from the case at  $S = 0.2$ , the vortex structures do not appear to break down in the higher region of the jet. Instead, the flow pattern becomes dominated by the periodic shedding of rib vortices.

The central vortex core is found with a columnar structure for the first two diameters after the exit. The interaction with the helical vortices results in a helical shape of the columnar vortex in the upper region of the jet. This is a precessing vortex core (PVC) phenomenon that appears as a precursor to the vortex breakdown as recently observed at similar swirl number by Markovich et al. (2014). While the vortex core is still too weak to induce negative velocities on the jet axis, in correspondence of the region in which the columnar vortex assumes an helical shape a low speed region is identified.

After three diameters from the exit the PVC seems to rapidly weaken. Although this could be associated to the conservation of angular momentum with the increase of cross section (negative vortex stretching), this sudden disappearance of the PVC is ascribed to the interaction with the rib vortices as visualized in data animations.

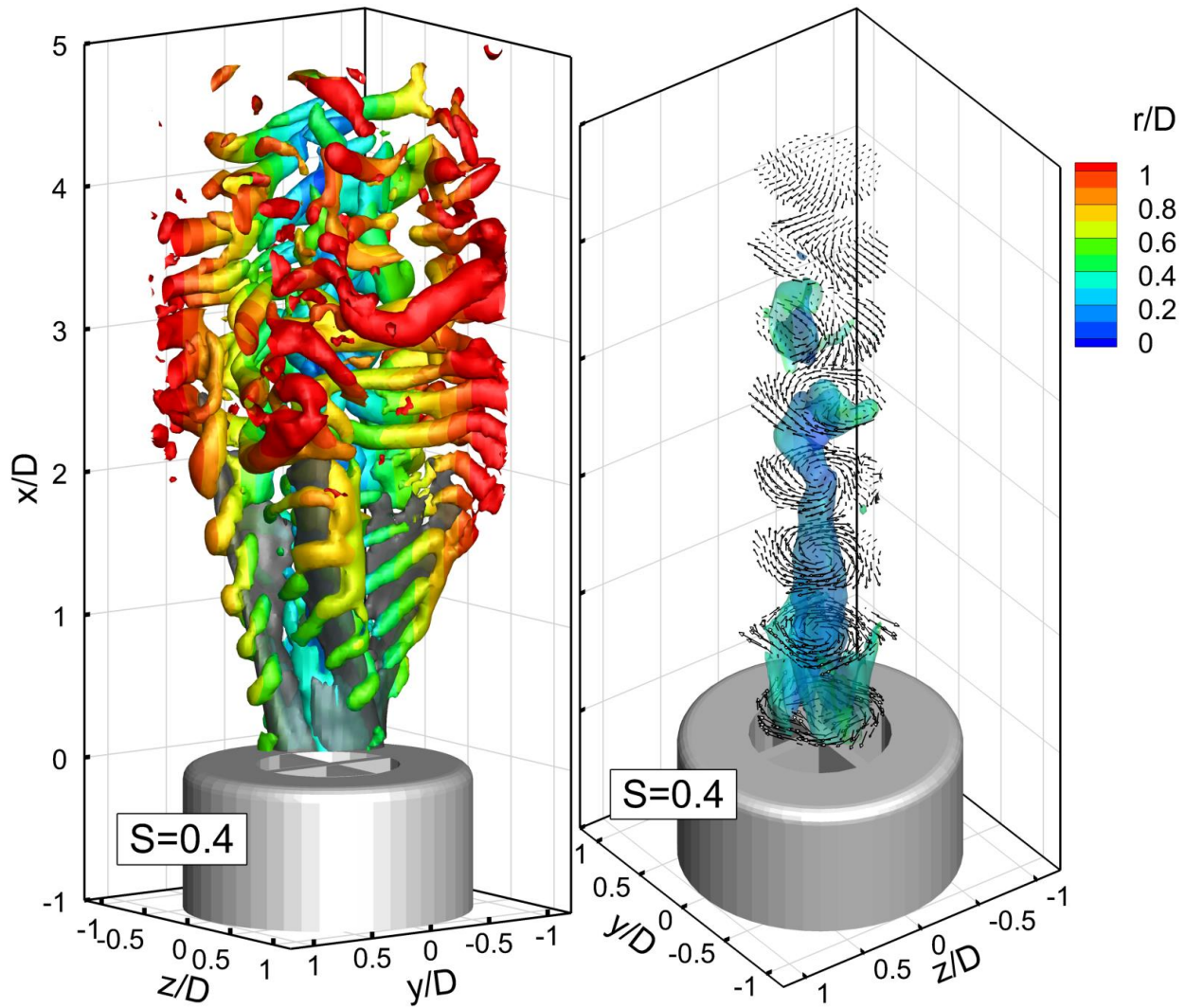


Fig. 3 Instantaneous flow organization at  $S = 0.4$ . Left: axial velocity and vortex topology. Isosurfaces and coloring identical to previous figure. Right: view of vortex core at  $r/D < 0.5$  with isosurface of axial vorticity and vectors projected along the  $y$ - $z$  axis.

### 3.2 Swirl jet in the core breakdown regime

Increasing  $S$  from 0.4 to 0.6 corresponds to further broadening the jet; as such helical vortices (who are expected to have the same streamwise pitch around the jet inserts) appear now as rib-like structures visible on the outer side of the jet sectors, which connect to weaker vortices on the inner side of the a jet. Further upwards, the vortices establish the azimuthal direction. The rib-vortices do not appear to undergo regular pairing, although the interaction occasionally leads to larger and more coherent vortices in the upper region of the jet. A surrogate of vortex pairing is also observed at  $S = 0.6$  as the result of interaction between rib-like vortices emanating from the jets of each sector. The onset of larger vortices with extended azimuthal coherence is observed starting from approximately 3 diameters from the jet exit. From these observations the swirling motion does not seem to suppress vortex pairing as instead seen by Panda and McLaughlin (1994), but rather anticipated at an upstream location as the swirl number is increased. This is consistent with the work by Liang and Maxworthy (2005) who observed vortex pairing at values of  $S$  above 1.

The central vortex core has increased with respect to the case at  $S = 0.4$ . The vortex features an overall axial pattern and is later formed by a double-helical structure. In fact, the columnar vortex core, at a distance of about 1.2 diameters from the nozzle breaks in a double helix in agreement with Sarpakaya (1971). A bubble

of recirculating fluid remains with a quasi-axisymmetric shape. The PVC appears to be dominated by helical vortex filaments fed by the inner shear layers of the jets from the vanes.

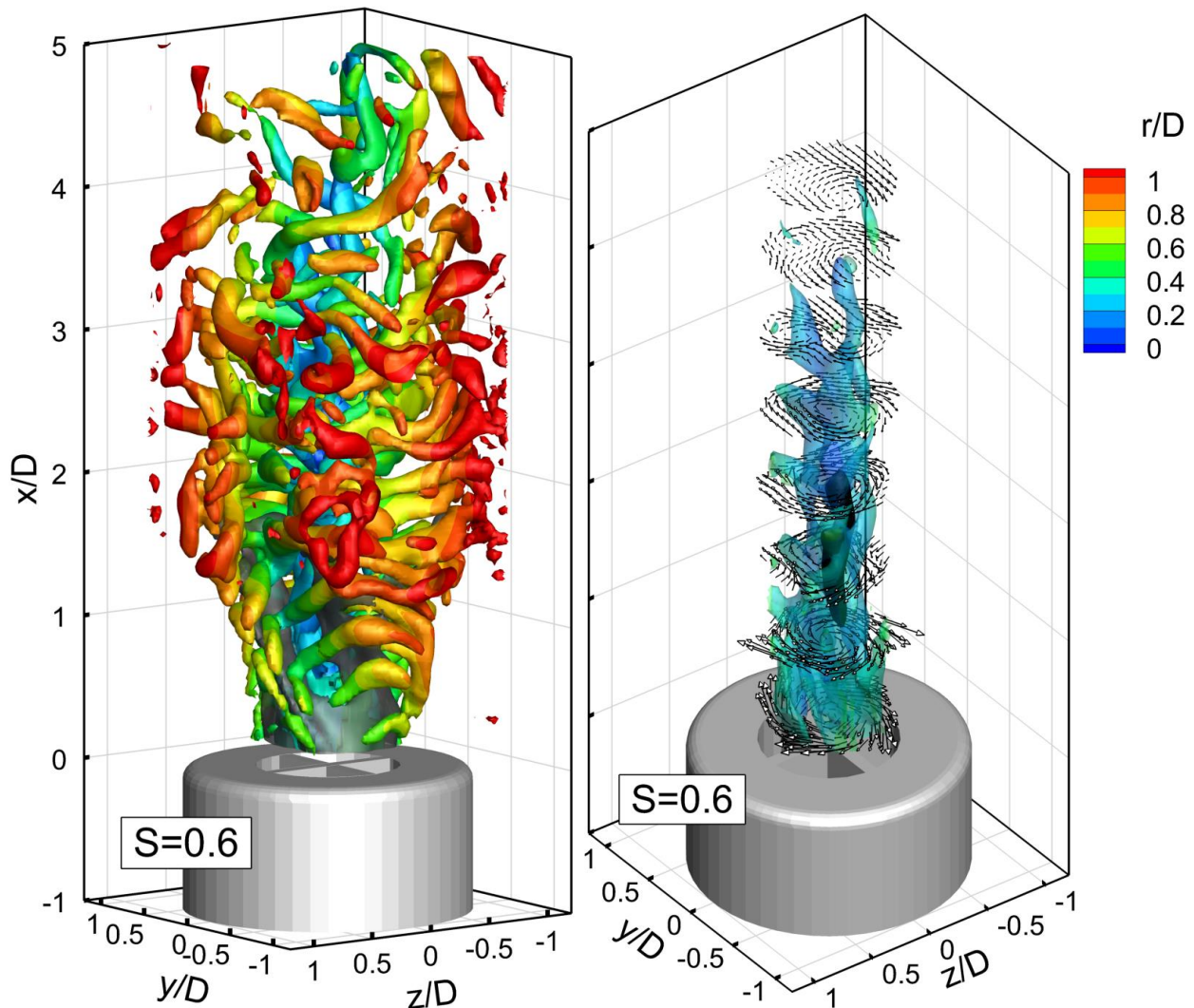


Fig. 4 Instantaneous flow organization at  $S = 0.6$ . Left, axial velocity and vortex topology. Right: view of vortex core at  $r/D < 0.5$  with isosurface of axial vorticity and vectors projected along the  $y$ - $z$  axis. A black isosurface indicates reverse flow ( $u/U = -0.1$ )

#### 4 Conclusions

The flow organization in swirling jets at moderate Reynolds has been inspected by time-resolved tomographic PIV. Cases at swirl number from 0.2 to 0.6 have been illustrated. The tomographic PIV technique is well suited to represent the complex three-dimensional vortex topology and the role of outer shear layer and inner core could be elucidated from the visualizations.

The overall jet organization is strongly dependent upon the four-vanes geometry used to impart the swirl. As a result the flow at the exit features four distinct jets.

The activity of the outer shear layer at  $S = 0.2$  is dominated by Kelvin-Helmholtz vortices with helical pattern. The latter appear to form double helices around each of the jets formed by the vanes. The pairing phenomenon is very clearly observed and its occurrence is anticipated increasing the swirl.

A transition from low-swirl ( $S < 0.4$ ) to high-swirl, is marked by a more pronounced activity of the precessing vortex core, which seems to be arranged with double helices.

## References

- [1] Lilley, D.G. (1977). Swirl flows in combustion: a review. *AIAA J.* 15, 1063.
- [2] Candel, S., Durox, D., Schuller, T., Bourgoign, J. F., & Moeck, J. P. (2014). Dynamics of swirling flames. *Annu. Rev. Fluid Mech.* 46, 147-173.
- [3] Harvey, J.K. (1962). Some observations of the vortex breakdown phenomenon. *J. Fluid Mech.* 14, 585.
- [4] Chigier, N.A. & Chervinsky, A. (1967). Aerodynamic study of turbulent burning free jets with swirl. *International Symposium on Combustion* 11, 489.
- [5] Billant, P., Chomaz, J.M. & Huerre P. (1998). Experimental study of vortex breakdown in swirling jets. *J. Fluid Mech.* 376, 183.
- [6] Rose W.G. (1962). A swirling round turbulent jet. *J. Appl. Mech.* 29, 615.
- [7] Gupta, A.K., Lilley, D.G. & Syred, N. (1984). *Swirl flows*. Kent Engl: Abacus.
- [8] Park, S.H. & Shin, H.D. (1993). Measurements of entrainment characteristics of swirling jets. *Int. J. Heat Mass Transfer* 36, 4009.
- [9] Harvey, J.K. (1962). Some observations of the vortex breakdown phenomenon. *J. Fluid Mech.* 14, 585.
- [10] Lucca-Negro, O. & O'Doherty, T. (2001). Vortex breakdown: a review. *Progress in Energy and Combustion Science* 27, 431.
- [11] Chanaud, R.C. (1965). Observations of oscillatory motion in certain swirling flows. *J. Fluid Mech.* 21, 111.
- [12] Syred, N. & Beer, J. M. (1974). Combustion in swirling flows: A review. *Combustion And Flame* 23, 143.
- [13] Yazdabadi, P.A. Griffiths, A.J. & Syred, N. (1994). Characterization of the PVC phenomena in the exhaust of a cyclone dust separator. *Exp.Fluids* 17, 84.
- [14] Syred, N. (2006). A review of oscillation mechanisms and the role of the precessing vortex core (PVC) in swirl combustion systems. *Progress in Energy and Combustion Science* 32, 93.
- [15] Martinelli, F. Olivani, A. & Coghe, A. (2007). Experimental analysis of the precessing vortex core in a free swirling jet. *Exp. Fluids* 42, 827.
- [16] Cala, C.E. Fernandes, E.C. Heitor, M.V., & Shtork, S.I. (2006). Coherent structures in unsteady swirling jet flow. *Exp.Fluids* 40, 267.
- [17] Oberleithner, K., Sieber, M., Nayeri, C.N., Paschereit, C.O., Petz, C., Hege, H.-C., Noack, B.R., & Wygnanski, I. (2011). Three-dimensional coherent structures in a swirling jet undergoing vortex breakdown: stability analysis and empirical mode construction. *J. Fluid Mech.* 679, 383–414.
- [18] Markovich, D.M., Abdurakipov, S.S., Chikishev, L. M., Dulin, V.M. & Hanjalić, K. (2014). Comparative analysis of low-and high-swirl confined flames and jets by proper orthogonal and dynamic mode decompositions. *Physics of Fluids* 26, 065109.
- [19] Ceglia, G., Discetti, S., Ianiro, A., Michaelis, D., Astarita, T., & Cardone, G. (2014). Three-dimensional organization of the flow structure in a non-reactive model aero engine lean burn injection system. *Experimental Thermal and Fluid Science* 52, 164-173.
- [20] Elsinga, G.E., Scarano, F., Wieneke, B. & van Oudheusden B.W. (2006). Tomographic particle image velocimetry, *Exp. Fluids* 41, 933-947.
- [21] Violato, D., & Scarano, F. (2011). Three-dimensional evolution of flow structures in transitional circular and chevron jets, *Physics of Fluids* 23, 124104.
- [22] Hunt, J.C.R., Wraya, A. & Moin, P. (1988). Eddies, stream, and convergence zones in turbulent flows.

Center for Turbulence Research Report CTR-S88, 193.

- [23] Jeong, J. & Hussain, F. (1995). On the identification of a vortex. *J. Fluid Mech.* 285, 69.
- [24] Scarano, F. (2013). Tomographic PIV: principles and practice. *Meas. Sci. Technol.* 24, 012001.
- [25] Novara, M., Batenburg, K.J. & Scarano, F. (2010). Motion tracking-enhanced MART for tomographic PIV. *Meas. Sci. Technol.* 21, 035401.
- [26] Lynch, K.P. & Scarano, F. (2010). A high-order time-accurate interrogation method for time-resolved PIV. *Meas. Sci. Technol.* 24, 035305.
- [27] Lynch, K.P. & Scarano, F. (2015). An efficient and accurate approach to MTE-MART for time-resolved tomographic PIV
- [28] Wieneke, B. (2008). Volume self-calibration for 3D particle image velocimetry. *Exp. Fluids* 45, 549-556.
- [29] Violato, D., Ianiro, A., Cardone, G. & Scarano, F. (2012). Three-dimensional vortex dynamics and convective heat transfer in circular and chevron impinging jets. *Int. J. Heat Fluid Flow* 37, 22-36.